 https://doi.org/10.3311/PPch.22771

Periodica Polytechnica Chemical Engineering, 67(4), pp. 592–602, 2023

Preparation of Highly Porous Scaffolds with Controllable Pore Size from Microbial Polyesters

Péter Polyák[1,2*], Ágoston Tóth[1,2], Dóra Tátraaljai[1,2]

[1] Laboratory of Plastics and Rubber Technology, Department of Physical Chemistry and Materials Science, Faculty of Chemical Technology and Biotechnology, Budapest University of Technology and Economics, Műegyetem rkp. 3., H-1111 Budapest, Hungary
[2] Institute of Materials and Environmental Chemistry, Research Centre for Natural Sciences, Magyar Tudósok Körútja 2., H-1117 Budapest, Hungary
[*] Corresponding author, e-mail: polyak.peter@vbk.bme.hu

Received: 11 June 2023, Accepted: 08 September 2023, Published online: 10 October 2023

Abstract

Microbial polyesters saw limited use in the field of tissue engineering, even though the biocompatibility of these polymers makes them ideal candidates for this role. The primary factor that hinders the proliferation of microbial polyesters in this market is that their processing with conventional techniques, such as electrospinning or 3D printing, is challenging. However, the full potential of these biopolymers could still be utilized by applying unconventional manufacturing methods, such as those based on the concept of salt leaching. An implementation of this concept facilitates the production of scaffolds that simultaneously have high porosity and excellent permeability. Moreover, the average pore size can also be varied in the range from 50 to 400 μm, which was reported to be optimal for the cultivation of eucaryotic cell cultures. By adjusting the pore size, the scaffold can be tailored to the eucaryotic cells the tissue consists of. Furthermore, we have developed an entirely new computational method for the approximation of the pore size distribution of the scaffolds. The method relies on 3D data reconstructed by the software of a digital optical microscope and also facilitates the modeling of the average pore size of scaffolds. Thus, besides the control of the pore size, our method enables its prediction as well.

Keywords

PHB-HV, microbial polyester, scaffold, tissue engineering, DOM

1 Introduction

One of the primary objectives of contemporary macromolecular science is the transition of the polymer industry toward a sustainable model. As a result of this effort, many polymer families emerged as potential alternatives for their fossil resource-based counterparts, such as polyolefins. A promising new family of polymers is that of microbial polyesters, which are natively synthesized by certain bacterial strains [1, 2]. In the living cell, these macromolecules are present in intracellular inclusions and are utilized by the bacteria as temporary material and energy storage [3]. Since the cells synthesize the macromolecules directly, the fermentation yields the polyester in one step. In contrast, polylactic acid (PLA) – the most relevant competitor of microbial polyesters – is synthesized in two steps, as the fermented organisms produce the monomer (lactic acid) only [4, 5]. Polymerization, which is the most challenging step of PLA production, is to be done in a subsequent step [4, 5].

A further advantage of microbial polyesters is that they can be fermented using several types of biomasses as a substrate. Besides carbohydrates [6], lipids may also be used for this purpose [7]. In order to reduce their prices and to make microbial polyesters more competitive in the market, several research projects targeted their production based on material sources available as side products of other industries. Examples include crude glycerol, a byproduct of the biodiesel industry [8], and lignin, produced in vast volumes by the timber and paper industry [9]. Recent studies have also demonstrated that these biopolymers can be fermented using materials originating from waste, such as agricultural waste [10], kitchen waste [11], or even wastewater [12]. As a result, the price of microbial polyesters was reduced to the range of $4–6/kg (i.e., five to six times that of polyolefins) and is expected to decrease even further [13]. Owing to their comparatively low price, microbial polyesters started to become popular

Cite this article as: Polyák, P., Tóth, Á., Tátraaljai, D. "Preparation of Highly Porous Scaffolds with Controllable Pore Size from Microbial Polyesters", Periodica Polytechnica Chemical Engineering, 67(4), pp. 592–602, 2023. https://doi.org/10.3311/PPch.22771

in industrial fields that output low added value products, such as the packaging industry [14]. Besides their competitive price, the relevance of these polyesters as a packaging material is due to their mechanical properties, which are similar to those of conventional polyolefins [15].

Microbial polyesters are not simply a mere alternative to polyolefins; their unique properties enable their application in fields where polyolefins cannot be used. Their excellent biocompatibility, for instance, makes them popular in the biomedical industry [16]. The past decade saw their *in vivo* application as orthopedic pins, stents, cardiovascular patches, tendon repair devices, or nerve guides [17]. Since microbial polyesters have already proliferated in the biomedical industry, researchers working in other fields also started to show interest in these materials. An important example is tissue engineering, which extensively uses biopolymers as materials for scaffold production [18]. The list of the most relevant examples includes PLA [19, 20], PGA (polyglycolic acid) [21], PCL (polycaprolactone) [22], PEG (polyethylene glycol) [23], as well as collagen [24], and gelatin [25]. Since several of the polymers listed above are polyesters (PLA, PGA, and PCL), microbial polyesters appear to be ideal candidates for this role.

Interestingly, microbial polyesters are still very rarely used for the production of scaffolds. The cause of the apparent lack of microbial polyesters in tissue engineering is not related to their hydrophobicity: each polyester listed above (PLA, PGA, and PCL) is hydrophobic, which seemingly contradicts their popularity in this scientific field. The reason why the hydrophobic nature of polyesters does not impede their utilization as scaffolds is that there are many, readily available techniques that can alter the surface characteristics of polyesters. The list of examples includes plasma treatment, UV irradiation, coating, or blending with other polymers [26–28]. Each method can be used for the hydrophilization of the surface of the macromolecular matrix, which paves the way before the application of polyesters as scaffolds. Consequently, the cause of the limited application of microbial polyesters in tissue engineering lies elsewhere.

The primary factors that severely limit the relevance of microbial polyesters in this field originate from the technical difficulties related to the method of manufacturing. For example, one of the most popular methods for scaffold production is electrospinning [29, 30]. Unfortunately, the production of electrospun fibers from microbial polyesters is hampered by multiple factors. For example, one of the most relevant microbial polyesters is poly(3-hydroxybutyrate) (PHB), which can be dissolved in only a limited number of solvents, such as halogenated alkanes, e.g., chloroform. Due to the large dipole moment of both the solvent and the polymer, strong dipole-dipole interactions dominate the liquid phase, which increases viscosity and leads to bead formation during electrospinning [31]. The problem of high viscosity could be addressed by the reduction of the concentration of the polymer. However, the average molecular weight of microbial polyesters is often significantly smaller than that of synthetic polymers [32]. As a result, at concentrations small enough to avoid bead formation, fibers cannot be produced at all.

A possible workaround for electrospinning-specific difficulties is the change of manufacturing technique. Scaffolds are often produced by 3D printing as well, mainly because in this way, the morphology of the product can be controlled very precisely [33]. A drawback of this method is that the most frequently used FDM (fused deposition modeling) printers build the scaffold layer by layer, i.e., successive layers have to be laid on the previous one. Construction of layers not having any support from below is not possible. As a result, 3D-printed scaffolds generally have low porosity [34–36], which is reduced even further if the printed polymer has a low molecular weight. Therefore, 3D printing of biopolyesters is technically possible, but the resulting scaffold will have especially low porosity. Since cells need space to reproduce themselves, the 3D-printed scaffolds presented in these articles [34–36] have questionable efficiency. Foam formation with a direct (chemical foaming [37], physical foaming with supercritical CO_2 [38]), or indirect (freeze-drying [39]) method could also be possible. However, the creation of open-cell foams from polyesters of low molecular weight, such as microbial polyesters, is challenging. Some researchers successfully addressed the problem by using chain extenders (e.g., epoxy-based styrene-acrylic oligomers [40]), but such additives worsen the biocompatibility of the product considerably.

In this paper, we would like to propose an alternative method for manufacturing scaffolds. Our technique is based on the concept of salt leaching, which was reported previously by Wang et al. [41], Amaro et al. [42], and Phuegyod et al. [43] to be an efficient tool for the creation of scaffolds from microbial polyesters. As proven by the results of these authors, the concept of salt leaching can be used to address each difficulty outlined above. Firstly, the technique works well with microbial polyesters, even if the raw polymer is of low molecular weight. Secondly, the resulting scaffolds are highly porous and have excellent permeability. Several researchers reported that the optimal pore size for cultivating eucaryotic cells ranges from 50 to 400 μm [44–47].

We will demonstrate that the average pore size of the microbial polyester can be adjusted and set to a desired value in the 50–400 μm range.

2 Experimental

2.1 Preparation of the scaffolds

The polymer (poly(3-hydroxybutyrate-co-3-hydroxyvalerate), PHB-HV) was purchased from TianAn Biopolymer; the product (Enmat Y1000P) was used without further purification. PHB-HV was dissolved in chloroform (Molar Chemicals Ltd.) at the boiling point of the solvent; the dissolution lasted an hour under constant reflux and stirring at 300 rpm. Solutions of five different concentrations (3.0, 3.5, 4.0, 4.5, and 5.0 m/m%) were prepared. As a pore former, sodium chloride (Molar Chemicals Ltd.) was used. Fractions of the salt were prepared with a sequence of sieves; the sieves had the following mesh sizes: 50, 100, 200, 300, 400, and 500 μm. The sieves were stacked in order of increasing mesh size, with the smallest at the bottom and the largest at the top. Then, polydisperse particles of sodium chloride were loaded onto the uppermost sieve (500 μm mesh size). The stack was placed on a sieve shaker that maintained constant vibration for 30 minutes. Subsequently, the stack was disassembled, and the fractions (50–100, 100–200, 200–300, 300–400, and 400–500 μm particle size) were removed from the sieves.

As the next step, the solution of the polymer and the fractions of the salt were mixed in order to form suspensions. In each case, 4 g salt was added to 8 mL of the solution, regardless of the average particle size of the fraction. The suspension was homogenized by stirring and subsequently poured into a rectangular metal frame measuring 5 cm in both width and length. Due to its high viscosity, the suspension had to be manually dispersed with a glass plate in order to ensure that the thickness of the suspension does not depend on the spatial coordinate. The complete evaporation of chloroform required a minimum of 15 hours and was carried out overnight. The next day, the samples were removed from the metal frame and placed into water which was stirred at 50 rpm. At room temperature, the complete dissolution of sodium chloride (i.e., the removal of the salt from the pores) required a minimum of 2 hours. Lastly, the samples were removed from the dissolution bath, washed with distilled water, and dried.

2.2 Analysis of macroscopic properties

Mechanical properties were characterized by tensile testing with an Instron 34SC-05 machine. Each measurement was carried out at 1 mm/min crosshead velocity and 30 mm gauge length. The porosity of the samples was determined using the water saturation method. The dry mass of the sample and its mass when fully saturated with water were recorded. The mass of the saturated sample was measured immediately after its removal from the dissolution bath. The difference between these values yields the mass of the imbibed water, which can be used to calculate the volume of the water contained by the pores. The volume of the polymer was calculated by dividing its dry mass by the density of PHB-HV, which is approximately 1.2 g/cm^3. Porosity was calculated by dividing the volume of water (i.e., volume of the air in dry scaffolds) by the total volume (volume of the air + volume of the polymer). Permeability was determined by measuring the volumetric flow rate of water through the scaffold. The sample was placed into a Büchner funnel, in which a constant level of water (1 cm) was maintained. The constant hydrostatic pressure (98.1 Pa) ensured a constant volumetric flow rate, which was calculated by measuring the time that was required for a pre-determined volume of water to pass through the membrane (80 mL). Dividing this volume with the measured time yields the targeted volumetric flow rate.

2.3 Analysis of microscopic structure and pore size

The microscopic structure of the scaffolds was analyzed by a digital optical microscope (DOM). For this purpose, a Keyence VHX 5000 DOM was used. Besides taking two-dimensional pictures, the instrument is also capable of the three-dimensional reconstruction of the surface of the sample. The reconstructed 3D surface consists of the highest points of the scaffold measured at each investigated X-Y coordinate pair. Note that even though the software of the DOM outputs 3D data, this method is limited to the investigation of the highest points of the scaffold because visible light cannot enter the polymer. Despite the lack of information from the lower layers of the scaffold, the 3D surface data can still be used for the estimation of not only the average pore size, but the pore size distribution as well. Pore size distribution was estimated from 3D data using a purpose-specific MATLAB software [48] developed by our research team.

3 Results and discussion

The results are discussed in Sections 3.1, 3.2, and 3.3. First, the microscopic structure and the macroscopic properties of the scaffolds will be presented. Section 3.1 will focus on properties relevant to the field of tissue engineering.

We will demonstrate that the scaffolds are highly porous and have excellent permeability, indicating their suitability for cell cultivation. Then, 3D data and the estimated pore size distributions will be presented and analyzed. Lastly, we will prove that with our method, the control of average pore size also becomes possible.

3.1 Microscopic structure and macroscopic properties of the scaffolds

Fig. 1 demonstrates that the factor that primarily influences the microscopic appearance of the scaffold is the average particle size of the salt fraction that was used for the creation of the sample. Fig. 1 compares the DOM images of samples created with 50–100 µm (Fig. 1(a)), 200–300 µm (Fig. 1(b)), and 400–500 µm (Fig. 1(c)) fractions and highlights that the structure changes drastically.

In contrast, the other investigated independent variable (concentration of the polymer) has little effect on the microscopic structure. The comparison of Fig. 1(c) and (d) demonstrates that scaffolds created from solutions having the lowest (3.0 m/m%; see Fig. 1(c)) and the highest (5.0 m/m%; see Fig. 1(d)) concentration have very similar microscopic appearances if the salt fraction used for the creation of the suspension was the same. We may conclude, therefore, that the structure of the scaffold can be controlled by varying the size of the particles. Fig. 1(a), (b), and (c) also reveal that the average pore sizes can span one order of magnitude, ranging from 50 to 500 µm. As mentioned in the introduction, this range of pore sizes has been reported in several studies to be optimal for the growth of eukaryotic cells [44–47].

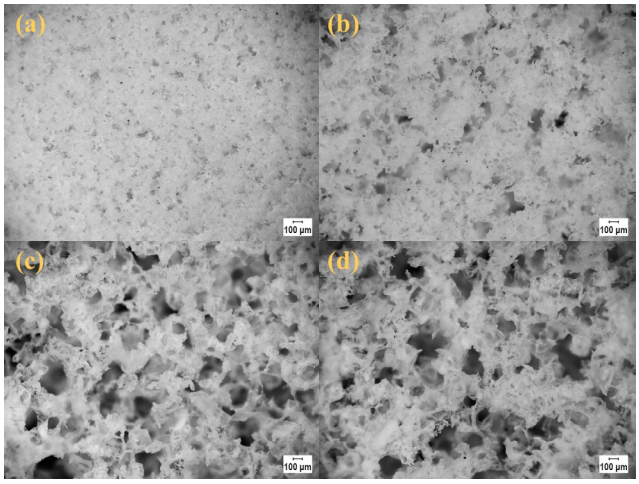

Fig. 1 Microscopic structure of scaffolds made with particle fractions of (a) 50–100 µm; (b) 200–300 µm; (c) 400–500 µm and (d) 400–500 µm. Samples in (a), (b), and (c) were prepared from solutions with a 3 m/m% polymer content. In contrast, the scaffold in (d) was produced using a solution with a 5 m/m% polymer content

Although the DOM images presented above suggest that the microscopic structure of these scaffolds is optimal for the purpose of engineering eukaryotic tissues, they also raise a few concerns. For example, Fig. 1 indicates that the porosity of the membranes is high, which can be associated with insufficient mechanical properties. Therefore, we also analyzed the mechanical characteristics and would like to present the results in order to prove that these scaffolds can fulfill their roles even if they have to withstand mechanical stress.

As mentioned above, the microscopic structure of the scaffolds is barely affected by the concentration of the polymer. In comparison, the investigated mechanical properties (tensile strength and modulus; see Fig. 2) appear to depend mainly on the concentration. Fig. 2 also highlights that the mechanical properties can be improved considerably by increasing the concentration of the polymer: there is an exponential correlation between these two. Consequently, in application areas where mechanical properties do not play an important role (e.g., *in vitro* studies),

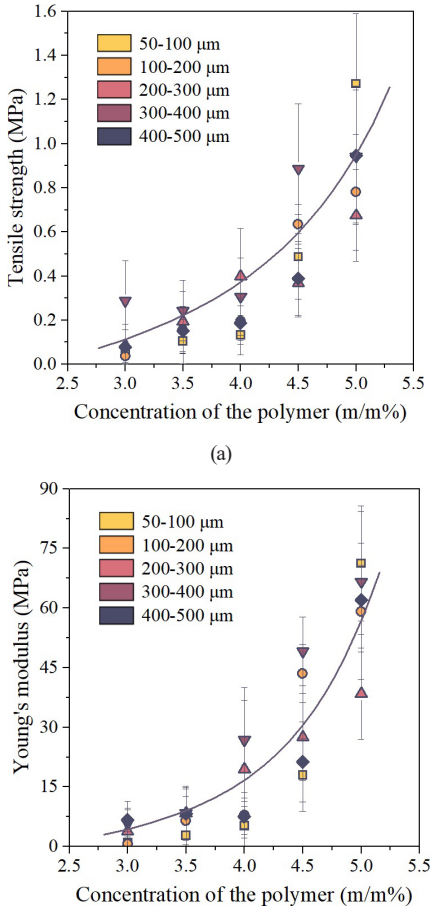

Fig. 2 Tensile strength (a) and modulus (b) of the scaffolds. Note that the mechanical properties can be improved considerably by raising the concentration of the polymer

the concentration of the polymer may be set to a low value in order to maximize porosity. Conversely, a significant proportion of scaffolds are employed *in vivo*, where they must withstand the mechanical stress exerted by the movement of the living body. Therefore, if the scaffold is intended to be used *in vivo*, raising the concentration of the polymer is strongly recommended. Above 4.0–4.5 m/m% concentration, the tensile strength can approach 1 MPa (Fig. 2(a)), which is an outstanding value for a highly porous scaffold.

3.2 Suitability for cell cultivation

In the field of tissue engineering, scaffolds have to meet several requirements. The optimal pore size and structural integrity discussed in Section 3.1 are necessary but not sufficient attributes. For instance, a considerable portion of the scaffolds described in the literature exhibit questionable efficiency due to their low porosity, i.e., most of the space in the scaffold is already occupied by the polymer [34–36]. 3D-printed scaffolds are especially prone to difficulties arising from insufficient porosity. Therefore, while developing our method of scaffold manufacturing, we paid special attention to the maximization of this parameter. The success of this effort is empirically proven by the data shown in Fig. 3.

The porosity correlates negatively with the concentration of the polymer, i.e., if the sample is created from a solution of increased polymer concentration, the resulting scaffold is expected to be less porous. Increasing the concentration of the polymers bears practical significance because in this way, the mechanical properties can be improved considerably (see Fig. 2). However, even if the concentration is maximized at the highest concentration we investigated and recommend (5 m/m%), the porosity remains above 90%. These findings indicate that the technology and sample preparation protocols proposed here are very robust: scaffolds of high porosity will be obtained, regardless of the concentration of the polymer used during the fabrication of the samples.

Another challenge frequently encountered by researchers aiming at the creation of scaffolds is related to the permeability of the scaffolds or, more precisely, the lack thereof. Insufficient permeability plagues scaffolds manufactured with any of the vast number of techniques based on foaming. In these products, the porosity is generally sufficient. However, cells can hardly penetrate the scaffold because, on the spectrum ranging from open-cell to closed-cell foams, the scaffold leans closer to the latter. Our concept, on the other hand, not only outperforms 3D printing but is also superior to foaming-based methods. In order to support the claims regarding the outstanding permeability of our scaffolds, this parameter was also quantitatively characterized; see Fig. 4.

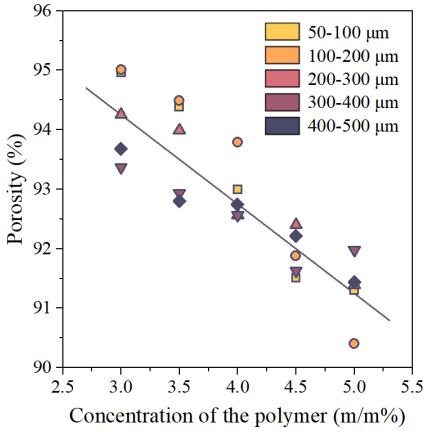

Fig. 3 Porosity of the scaffolds plotted against the concentration of the solution. The porosity stays above 90%, even if the scaffold was created from a 5 m/m% solution

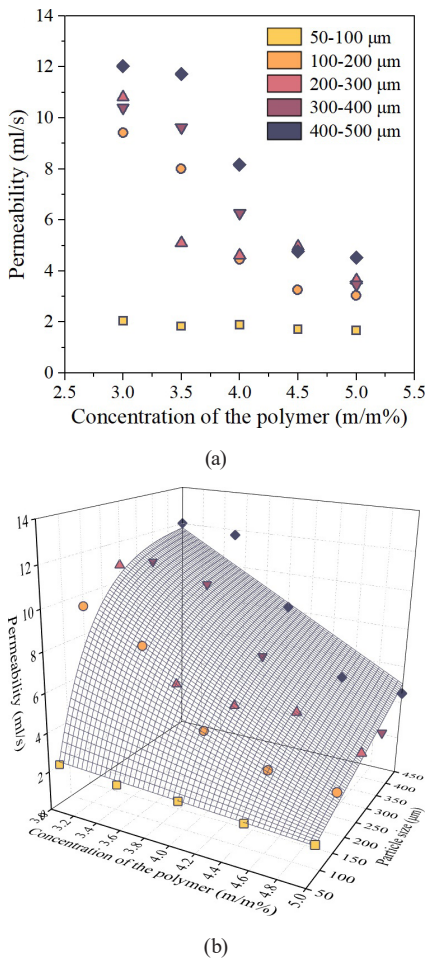

Fig. 4 Permeability of the scaffolds plotted against the concentration of the solution of the polymer (a) and against the concentration and the average size of particles (b)

Fig. 4(a) suggests that the concentration of the polymer and the permeability of the scaffold correlate negatively, i.e., scaffolds created from more concentrated solutions let through water with a lower volumetric flow rate. However, we also would like to emphasize that even in the case of scaffolds with the worst permeability, the volumetric flow rate maintained by the hydrostatic pressure of 1 cm water column is around 2 mL/s. In practice, this means that the scaffold can barely retain water; it can flow through the pores very easily. The second correlation we would like to highlight is that between the permeability and the average size of salt particles. Due to the stochastic errors that bias the measurement, this correlation is more difficult to represent graphically and may not be obvious at first sight.

Therefore, Fig. 4(b) was also created and is meant to prove that the permeability increases monotonously with the particle size of the pore former. By adjusting both independent variables, scaffolds with permeabilities as high as 12 mL/s can be created. The remarkable permeability demonstrated by Fig. 4(a) and (b) suggests that the proliferation of the cells in these scaffolds will not be sterically hindered.

3.3 Analysis and control of the pore size

The pore size and pore size distribution can be analyzed in many ways. As a part of this project, we decided to use an advanced feature of our digital optical microscope. Our DOM can measure the Z coordinate of the highest point of the sample at each X-Y coordinate pair. In simpler words, it can create and output a three-dimensional surface that consists of the highest points of the scaffold. An example of this surface is shown in Fig. 5. In order to estimate the distribution of pore sizes from the 3D data shown in this diagram, we will assume that the depth reached by the photons emitted by the light source of DOM correlates positively with the size of the void that enabled the photon to penetrate the scaffold. This is not necessarily true because the investigated surface of the scaffold was not created by cutting a scaffold in half.

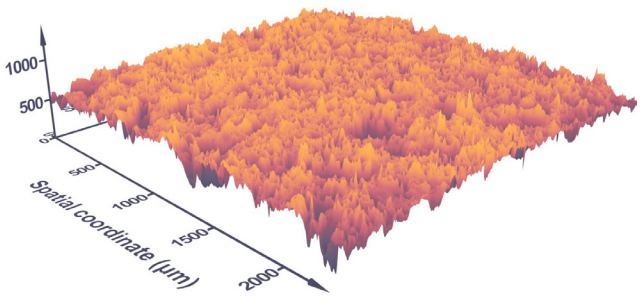

Fig. 5 Surface of a membrane reconstructed by the software of the digital optical microscope. The investigated sample was created from a 3 m/m% solution; as the pore former, the 100–200 µm fraction of the salt was used

Although the structure on the surface may not perfectly represent the rest of the scaffold, for the purpose of an approximative estimation, it is an adequate starting point. As the next step, we have to measure at each depth (i.e., at each Z coordinate) whether the photons reached that depth. For example, if the investigated Z value is close to the objective of the microscope, it is very probable that the photons successfully reach this level. The probabilities can be calculated by setting a plane to the investigated Z coordinate (see Fig. 6(a)) and comparing this Z coordinate to the Z coordinate of the 3D surface at every X-Y coordinate pair (see Fig. 6(d)) This comparison yields a surface function, which is integrated in the next computational step (see in Eq. (1)):

$$A_z = \int_{x_0}^{x_1}\int_{y_0}^{y_1} f_z(x,y)\,dxdy. \tag{1}$$

In Eq. (1), A_z is the total size of the area where the photons could not penetrate the membrane because they hit the surface of the polymer. $f_z(x,y)$ represents the surface function visualized in Fig. 6(d). The 'z' index indicates that the measured integral belongs to one particular Z height. x and y are the spatial coordinates attributed to the horizontal axes, whereas z is the spatial coordinate attributed to the axis being parallel with the direction of the photons. In the subsequent step, the plane is to be moved to a smaller Z value, indexed in Fig. 6 as $z = 2$. The comparison (Fig. 6(b)) yields the next $f_{z=2}$ function (Fig. 6(e)), which must be integrated (Eq. 1) in order to obtain the cumulative area ($A_{z=2}$). These steps are to be repeated again (Fig. 6(c) and (f)) until the bottom of the scaffold is reached.

The recursive computation of integrals yields a cumulated surface as a function of the Z coordinate; see the yellow curve in Fig. 6(g). At this point, we wish to point out again that depth of penetration (the investigated Z height in this context) can be used to approximate the size of the pore that enabled the photons to penetrate the scaffold. Although the surface of the scaffold does not perfectly represent its internal structure, it offers a reliable approximation since the pore size distribution does not depend on the distance from the surface. This assumption was confirmed by DOM micrographs of the cross-section, submitted in the Supplement. The similarity between the cross-section and the surface of the scaffold confirms our initial assumption, i.e., surface analysis yields quantitative data that represents the entire scaffold. Therefore, subsequent

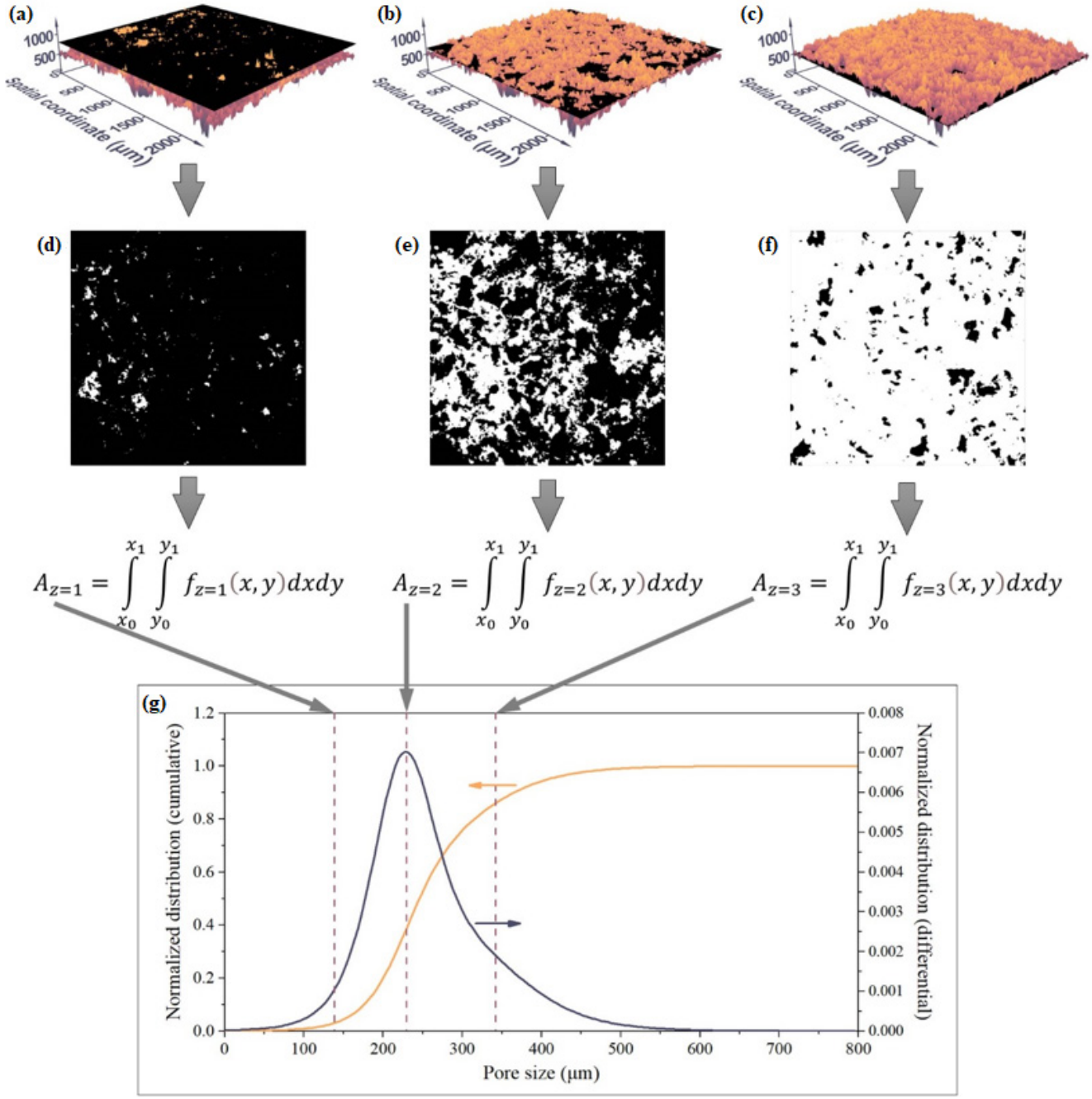

Fig. 6 Comparison of the 3D surface and the reference plane in (a) $z = 1$; (b) $z = 2$; and (c) $z = 3$ positions, as well as the result of the comparison carried out in (d) $z = 1$; (e) $z = 2$; and (f) $z = 3$ positions. (g) demonstrates the cumulative and differential curves that can be calculated from the results of surface analysis. The calculation was performed on a scaffold created from a 100–200 µm fraction of the pore former and a 3 m/m% solution of the polymer

computational steps can be based on the results of the surface scan. In the next step, the cumulative curve calculated by using the method discussed above may be derived in order to obtain the differential curve (plotted in grey in Fig. 6(g)), which can be used as an approximation of the pore size distribution.

The distribution of pore size was calculated for each membrane. As expected, the distribution is primarily determined by the particle size of the pore former (see Fig. 7(a)) and is not affected considerably by the concentration of the polymer. Fig. 7(a) also reveals that deviance from the normal distribution increases with increasing average pore size. While pore size distribution measured in the case of scaffolds created with the 50–100 µm salt fraction has an almost perfect Gaussian shape, samples with larger average pore sizes have increasingly asymmetric distribution functions. The distribution of the last sample (400–500 µm) is not only asymmetric but is also bimodal. These

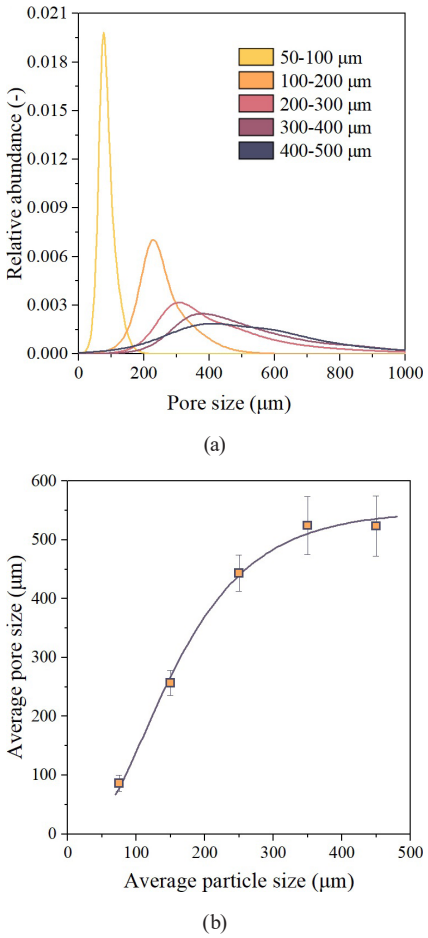

Fig. 7 Normalized distributions (a) and their averages plotted against the particle size of the pore former (b)

deviations shed light on the uncertainty inherent to the computational method demonstrated in Fig. 6. Despite all the shortcomings and limitations of the DOM-based pore size analysis, we found its application advantageous for multiple reasons. It can be performed rapidly; it is non-destructive and, most importantly, offers a straightforward method for the quantitative characterization of the correlation between the particle size of the pore former and the average pore size of the scaffold (see Fig. 7(b)).

The results presented in Fig. 7 can be compared to experimental data found in the literature. For instance, Gentile et al [49] developed scaffolds for cultivating eukaryotic cell cultures and utilized computer tomography (µ-CT) for the three-dimensional reconstruction of the porous samples. From the 3D data, the authors calculated the pore size distributions and presented the distribution functions alongside the three-dimensional micrographs [49]. The article reports pore sizes that range from 50 to 200 µm, whereas the maximum of the distribution functions varies between 126 and 175 µm. These values indicate that results that originate from µ-CT analysis align well with our data calculated for scaffolds created by using 50–100 µm and 100–200 µm fractions of the pore former.

Besides the coherence between our results and those available in the literature, we also would like to draw attention to an important tendency outlined by the regression curve presented in Fig. 7(b). The average pore size plotted on the vertical axis of Fig. 7(b) does not equal the position of the maximum of the peaks in Fig. 7(a) because the distribution functions are asymmetric to varying extents. We have found that plotting the averages (instead of the locations of the maxima) outlines a stronger correlation. Accordingly, for the modeling and prediction of the pore size of the scaffolds, the average pore sizes will be used; see Fig. 7(b). Fig. 7 also suggests that the correlation between the independent and dependent variables is strong, but nonlinear. Thus, the calculation of the regression is carried out with an exponential function; see the gray regression curve in Fig. 7(b) and Eq. (2).

$$D_s = a \times \left(1 - e^{-b \times D_p}\right)^c , \tag{2}$$

where D_s and D_p refer to the average pore size of the scaffold (hence the '*s*' index) and the average particle size of the pore former (hence the '*p*' index). *a*, *b*, and *c* are regression parameters that depend on the characteristics of the polymer and the solvent. In the case of our experiments, carried out with PHB-HV and chloroform, *a*, *b*, and *c* were calculated to equal 548.5 µm, 0.01107 1/µm, and 3.411 (–), respectively. Besides a mere graphical representation of a positive correlation, Fig. 7(b) also proves that the average pore size of the scaffold can be controlled by varying the particle size of the pore former. Furthermore, by modeling the positive correlation (see Eq. (2)), the average pore size of the scaffold can also be predicted. The procedure of prediction is as follows. First, a pore former is to be selected, e.g., fractions of sodium chloride. Then, the particle size of the pore former (D_p) is to be substituted into Eq. (2). With the help of the regression parameters (*a*, *b*, and *c*) already calculated and submitted above, the right-hand side of Eq. (2) can also be computed, which equals the targeted value, i.e., the average pore size of the scaffold.

4 Conclusions

Although the fabrication of scaffolds from microbial polyesters is challenging, the technical difficulties can be eliminated. A possible way of circumnavigating the roadblocks of method development is based on the utilization

of techniques that are introduced but sparsely applied in the field of tissue engineering. The method we propose relies on the concept of salt leaching, which, despite its potential, saw limited use for the purpose of scaffold creation from microbial polyesters. The results of our studies demonstrated that the implementation of this concept facilitates the production of scaffolds that are superior to their counterparts created with conventional techniques. Unlike scaffolds created with 3D printing, the ones presented in our paper have especially high porosity (>90%). Methods based on foaming or lyophilization yield scaffolds that often suffer from low permeability. In contrast, the scaffolds presented here were shown to have both high porosity and excellent permeability. Exceptionally high porosity and permeability could lead to poor mechanical performance. However, the measured mechanical properties allowed us to conclude that these products are capable of withstanding considerable mechanical stress. We have also proven that the technology is robust and works even with neat microbial polyesters, as opposed to electrospinning. As a last conclusion, we would like to highlight that with the help of our new computational method relying on the 3D surface data reconstructed by the DOM, the approximation of the pore size distribution also became possible. The success of these calculations has opened up new possibilities. For example, the quantitative characterization of the correlation between the particle size of the pore former and the average pore size of the scaffold can now be performed rapidly. Thus, our experimental procedure not only allows the control of the average pore size of the scaffold, but also facilitates the modeling and prediction of this parameter.

Acknowledgments

The National Research, Development and Innovation Fund of Hungary (OTKA PD 138430) is greatly acknowledged for the financial support of this research. The H2020-MSCA RISE No. 872152 - GREEN-MAP project of the European Union also provided financial support. Project no. TKP-9-8/PALY-2021 has been implemented with the support provided by the Ministry of Culture and Innovation of Hungary from the National Research, Development and Innovation Fund, financed under the TKP2021-EGA funding scheme.

References

[1] Zhou, W., Bergsma, S., Colpa, D. I., Euverink, G.-J. W., Krooneman, J. "Polyhydroxyalkanoates (PHAs) synthesis and degradation by microbes and applications towards a circular economy", Journal of Environmental Management, 341, 118033, 2023. https://doi.org/10.1016/j.jenvman.2023.118033

[2] Chavan, S., Yadav, B., Tyagi, R. D., Drogui, P. "A review on production of polyhydroxyalkanoate (PHA) biopolyesters by thermophilic microbes using waste feedstocks", Bioresource Technology, 341, 125900, 2021. https://doi.org/10.1016/j.biortech.2021.125900

[3] Obruca, S., Sedlacek, P., Mravec, F., Krzyzanek, V., Nebesarova, J., Samek, O., Kucera, D., Benesova, P., Hrubanova, K., Milerova, M., Marova, I. "The presence of PHB granules in cytoplasm protects non-halophilic bacterial cells against the harmful impact of hypertonic environments", New Biotechnology, 39, pp. 68–80, 2017. https://doi.org/10.1016/j.nbt.2017.07.008

[4] Swetha, T. A., Bora, A., Mohanrasu, K., Balaji, P., Raja, R., Ponnuchamy, K., Muthusamy, G., Arun, A. "A comprehensive review on polylactic acid (PLA) – Synthesis, processing and application in food packaging", International Journal of Biological Macromolecules, 234, 123715, 2023. https://doi.org/10.1016/j.ijbiomac.2023.123715

[5] Yu, J., Xu, S., Liu, B., Wang, H., Qiao, F., Ren, X., Wei, Q. "PLA bioplastic production: From monomer to the polymer", European Polymer Journal, 193, 112076, 2023. https://doi.org/10.1016/j.eurpolymj.2023.112076

[6] García, A., Segura, D., Espín, G., Galindo, E., Castillo, T., Peña, C. "High production of poly-β-hydroxybutyrate (PHB) by an *Azotobacter vinelandii* mutant altered in PHB regulation using a fed-batch fermentation process", Biochemical Engineering Journal, 82, pp. 117–123, 2014. https://doi.org/10.1016/j.bej.2013.10.020

[7] Obruca, S., Marova, I., Snajdar, O., Mravcova, L., Svoboda, Z. "Production of poly(3-hydroxybutyrate-*co*-3-hydroxyvalerate) by *Cupriavidus necator* from waste rapeseed oil using propanol as a precursor of 3-hydroxyvalerate", Biotechnology Letters, 32(12), pp. 1925–1932, 2010. https://doi.org/10.1007/s10529-010-0376-8

[8] Drusilla Wendy, Y. B., Nor Fauziah, M. Z., Siti Baidurah, Y., Tong, W. Y., Lee, C. K. "Production and characterization of polyhydroxybutyrate (PHB) BY *Burkholderia cepacia* BPT1213 using waste glycerol as carbon source", Biocatalysis and Agricultural Biotechnology, 41, 102310, 2022. https://doi.org/10.1016/j.bcab.2022.102310

[9] Tomizawa, S., Chuah, J.-A., Matsumoto, K., Doi, Y., Numata, K. "Understanding the Limitations in the Biosynthesis of Polyhydroxyalkanoate (PHA) from Lignin Derivatives", ACS Sustainainable Chemistry & Engineering, 2(5), pp. 1106–1113, 2014. https://doi.org/10.1021/sc500066f

[10] Sandhya, M., Aravind, J., Kanmani, P. "Production of polyhydroxyalkanoates from *Ralstonia eutropha* using paddy straw as cheap substrate", International Journal of Environmental Science and Technology, 10(1), pp. 47–54, 2013. https://doi.org/10.1007/s13762-012-0070-6

[11] Loan, T. T., Trang, D. T. Q., Huy, P. Q., Ninh, P. X., Van Thuoc, D. "A fermentation process for the production of poly(3-hydroxybutyrate) using waste cooking oil or waste fish oil as inexpensive carbon substrate", Biotechnology Reports, 33, e00700, 2022. https://doi.org/10.1016/j.btre.2022.e00700

[12] Muhorakeye, A., Cayetano, R. D., Kumar, A. N., Park, J., Pandey, A. K., Kim, S.-H. "Valorization of pretreated waste activated sludge to organic acids and biopolymer", Chemosphere, 303, 135078, 2022. https://doi.org/10.1016/j.chemosphere.2022.135078

[13] Tan, D., Wang, Y., Tong, Y., Chen, G.-Q. "Grand Challenges for Industrializing Polyhydroxyalkanoates (PHAs)", Trends in Biotechnology, 39(9), pp. 953–963, 2021. https://doi.org/10.1016/j.tibtech.2020.11.010

[14] Tripathi, A. D., Mishra, P. K., Darani, K. K., Agarwal, A., Paul, V. "Hydrothermal treatment of lignocellulose waste for the production of polyhydroxyalkanoates copolymer with potential application in food packaging", Trends in Food Science & Technology, 123, pp. 233–250, 2022. https://doi.org/10.1016/j.tifs.2022.03.018

[15] Briassoulis, D., Tserotas, P., Athanasoulia, I.-G. "Alternative optimization routes for improving the performance of poly(3-hydroxybutyrate) (PHB) based plastics", Journal of Cleaner Production, 318, 128555, 2021. https://doi.org/10.1016/j.jclepro.2021.128555

[16] Gregory, D. A., Taylor, C. S., Fricker, A. T. R., Asare, E., Tetali, S. S. V., Haycock, J. W., Roy, I. "Polyhydroxyalkanoates and their advances for biomedical applications", Trends in Molecular Medicine, 28(4), pp. 331–342, 2022. https://doi.org/10.1016/j.molmed.2022.01.007

[17] Zhang, J., Shishatskaya, E. I., Volova, T. G., da Silva, L. F., Chen, G.-Q. "Polyhydroxyalkanoates (PHA) for therapeutic applications", Materials Science and Engineering: C, 86, pp. 144–150, 2018. https://doi.org/10.1016/j.msec.2017.12.035

[18] Suamte, L., Tirkey, A., Babu, P. J. "Design of 3D smart scaffolds using natural, synthetic and hybrid derived polymers for skin regenerative applications", Smart Materials in Medicine, 4, pp. 243–256, 2023. https://doi.org/10.1016/j.smaim.2022.09.005

[19] Santoro, M., Shah, S. R., Walker, J. L., Mikos, A. G. "Poly(lactic acid) nanofibrous scaffolds for tissue engineering", Advanced Drug Delivery Reviews, 107, pp. 206–212, 2016. https://doi.org/10.1016/j.addr.2016.04.019

[20] Wang, C., Wang, H., Chen, Q., Gang, H., Zhou, Y., Gu, S., Liu, X., Xu, W., Zhang, B., Yang, H. "Polylactic acid scaffold with directional porous structure for large-segment bone repair", International Journal of Biological Macromolecules, 216, pp. 810–819, 2022. https://doi.org/10.1016/j.ijbiomac.2022.07.207

[21] Zhang, J., Song, C., Han, Y., Xi, Z., Zhao, L., Cen, L., Yang, Y. "Regulation of inflammatory response to polyglycolic acid scaffolds through incorporation of sodium tripolyphosphate", European Polymer Journal, 122, 109349, 2020. https://doi.org/10.1016/j.eurpolymj.2019.109349

[22] Fiedler, T., Videira, A. C., Bártolo, P., Strauch, M., Murch, G. E., Ferreira, J. M. F. "On the mechanical properties of PLC–bioactive glass scaffolds fabricated via BioExtrusion", Materials Science and Engineering: C, 57, pp. 288–293, 2015. https://doi.org/10.1016/j.msec.2015.07.063

[23] Khodaverdi, E., Reza Abbaspour, M., Oroojalian, F., Omidkhah, N., Hossein-nezahd, S., Kamali, H., Hadizadeh, F. "Dexamethasone delivery of porous PEG-PCL-PEG scaffolds with supercritical carbon dioxide gas foaming", Journal of Drug Delivery Science and Technology, 66, 102547, 2021. https://doi.org/10.1016/j.jddst.2021.102547

[24] Muran, A. C., Schaffler, B. C., Wong, A., Neufeld, E., Swami, P., Pianka, M., Grande, D. "Effect of increasing hyaluronic acid content in collagen scaffolds on the maintenance of chondrogenic phenotype in chondrocytes and mesenchymal stem cells", Journal of Cartilage & Joint Preservation, 3(2), 100099, 2023. https://doi.org/10.1016/j.jcjp.2023.100099

[25] Rashid, A. B., Showva, N.-N., Hoque, M. E. "Gelatin-based scaffolds: An intuitive support structure for regenerative therapy", Current Opinion in Biomedical Engineering, 26, 100452, 2023. https://doi.org/10.1016/j.cobme.2023.100452

[26] Ammosova, L., Jiang, Y., Suvanto, M., Pakkanen, T. A. "Selective three-dimensional hydrophilization of microstructured polymer surfaces through confined photocatalytic oxidation", Applied Surface Science, 329, pp. 58–64, 2015. https://doi.org/10.1016/j.apsusc.2014.12.147

[27] Yang, Y.-F., Li, Y., Li, Q.-L., Wan, L.-S., Xu, Z.-K. "Surface hydrophilization of microporous polypropylene membrane by grafting zwitterionic polymer for anti-biofouling", Journal of Membrane Science, 362(1–2), pp. 255–264, 2010. https://doi.org/10.1016/j.memsci.2010.06.048

[28] Kratz, K., Heuchel, M., Weigel, T., Lendlein, A. "Surface hydrophilization of highly porous poly(ether imide) microparticles by covalent attachment of poly(vinyl pyrrolidone)", Polymer, 210, 123045, 2020. https://doi.org/10.1016/j.polymer.2020.123045

[29] Ghosal, K., Agatemor, C., Špitálsky, Z., Thomas, S., Kny, E. "Electrospinning tissue engineering and wound dressing scaffolds from polymer-titanium dioxide nanocomposites", Chemical Engineering Journal, 358, pp. 1262–1278, 2019. https://doi.org/10.1016/j.cej.2018.10.117

[30] Ceretti, E., Ginestra, P. S., Ghazinejad, M., Fiorentino, A., Madou, M. "Electrospinning and characterization of polymer–graphene powder scaffolds", CIRP Annals, 66(1), pp. 233–236, 2017. https://doi.org/10.1016/j.cirp.2017.04.122

[31] Fong, H., Chun, I., Reneker, D. H. "Beaded nanofibers formed during electrospinning", Polymer, 40(16), pp. 4585–4592, 1999. https://doi.org/10.1016/S0032-3861(99)00068-3

[32] Mantzaris, N. V., Kelley, A. S., Daoutidis, P., Srienc, F. "A population balance model describing the dynamics of molecular weight distributions and the structure of PHA copolymer chains", Chemical Engineering Science, 57(21), pp. 4643–4663, 2002. https://doi.org/10.1016/S0009-2509(02)00370-6

[33] Mirkhalaf, M., Men, Y., Wang, R., No, Y., Zreiqat, H. "Personalized 3D printed bone scaffolds: A review", Acta Biomateriala, 156, pp. 110–124, 2023. https://doi.org/10.1016/j.actbio.2022.04.014

[34] Lee, J.-S., Cha, H. D., Shim, J.-H., Jung, J. W., Kim, J. Y., Cho, D.-W. "Effect of pore architecture and stacking direction on mechanical properties of solid freeform fabrication-based scaffold for bone tissue engineering", Journal of Biomedical Materials Research: Part A, 100A(7), pp. 1846–1853, 2012. https://doi.org/10.1002/jbm.a.34149

[35] Liu, X., Gaihre, B., Park, S., Li, L., Dashtdar, B., Astudillo Potes, M. D., Terzic, A., Elder, B. D., Lu, L. "3D-printed scaffolds with 2D hetero-nanostructures and immunomodulatory cytokines provide pro-healing microenvironment for enhanced bone regeneration", Bioactive Materials, 27, pp. 216–230, 2023. https://doi.org/10.1016/j.bioactmat.2023.03.021

[36] Rezaei, H., Matin, A. A., Vahdati-khajeh, S., Habibi, B. "3D printed solid phase microextraction scaffolds as novel tool for sample preparation; application in antifungal drugs analysis", Journal of Chromatography B, 1225, 123757, 2023. https://doi.org/10.1016/j.jchromb.2023.123757

[37] Krauss Juillerat, F., Gonzenbach, U. T., Elser, P., Studart, A. R., Gauckler, L. J. "Microstructural Control of Self-Setting Particle-Stabilized Ceramic Foams", Journal of the American Ceramic Society, 94(1), pp. 77–83, 2011. https://doi.org/10.1111/j.1551-2916.2010.04040.x

[38] Santos-Rosales, V., Magariños, B., Starbird, R., Suárez-González, J., Fariña, J. B., Alvarez-Lorenzo, C., García-González, C. A. "Supercritical CO_2 technology for one-pot foaming and sterilization of polymeric scaffolds for bone regeneration", International Journal of Pharmaceutics, 605, 120801, 2021. https://doi.org/10.1016/j.ijpharm.2021.120801

[39] Shuang, F.-F., Wang, C.-C., Zhu, W.-J., Chen, T., Yao, X.-H., Zhang, D.-Y., Zhao, W.-G. "Preparation of a robust silk fibroin scaffold with a reinforced concrete structure constructed with silk nanofibers as the skeleton based on a $CaCl_2$-formic acid solution and freeze-drying method", Polymer Testing, 111, 107599, 2022. https://doi.org/10.1016/j.polymertesting.2022.107599

[40] Ni, J., Yu, K., Zhou, H., Mi, J., Chen, S., Wang, X. "Morphological evolution of PLA foam from microcellular to nanocellular induced by cold crystallization assisted by supercritical CO_2", The Journal of Supercritical Fluids, 158, 104719, 2020. https://doi.org/10.1016/j.supflu.2019.104719

[41] Wang, N., Zhou, Z., Xia, L., Dai, Y., Liu, H. "Fabrication and characterization of bioactive β-Ca_2SiO_4/PHBV composite scaffolds", Materials Science and Engineering: C, 33(4), pp. 2294–2301, 2013. https://doi.org/10.1016/j.msec.2013.01.059

[42] Amaro, L., Correia, D. M., Martins, P. M., Botelho, G., Carabineiro, S. A. C., Ribeiro, C., Lanceros-Mendez, S. "Morphology Dependence Degradation of Electro- and Magnetoactive Poly(3-hydroxybutyrate-co-hydroxyvalerate) for Tissue Engineering Applications", Polymers, 12(4), 953, 2020. https://doi.org/10.3390/polym12040953

[43] Phuegyod, S., Pramual, S., Wattanavichean, N., Assawajaruwan, S., Amornsakchai, T., Sukho, P., Svasti, J., Surarit, R., Niamsiri, N. "Microbial Poly(hydroxybutyrate-co-hydroxyvalerate) Scaffold for Periodontal Tissue Engineering", Polymers, 15(4), 855, 2023. https://doi.org/10.3390/polym15040855

[44] Nam, J. H., Lee, S. Y., Khan, G., Park, E. S. "Validation of the optimal scaffold pore size of nasal implants using the 3-dimensional culture technique", Archives of Plastic Surgery, 47(4), pp. 310–316, 2020. https://doi.org/10.5999/aps.2020.00213

[45] Perez, R. A., Mestres, G. "Role of pore size and morphology in musculo-skeletal tissue regeneration", Materials Science and Engineering: C, 61, pp. 922–939, 2016. https://doi.org/10.1016/j.msec.2015.12.087

[46] Murphy, C. M., O'Brien, F. J. "Understanding the effect of mean pore size on cell activity in collagen-glycosaminoglycan scaffolds", Cell Adhesion & Migration, 4(3), pp. 377–381, 2010. https://doi.org/10.4161/cam.4.3.11747

[47] Loh, Q. L., Choong, C. "Three-Dimensional Scaffolds for Tissue Engineering Applications: Role of Porosity and Pore Size", Tissue Engineering Part B: Reviews, 19(6), pp. 485–502, 2013. https://doi.org/10.1089/ten.teb.2012.0437

[48] Mathworks "MATLAB, (R2023a)", [computer program] Available at: https://www.mathworks.com/products/matlab.html [Accessed: 16 February 2023]

[49] Gentile, P., Mattioli-Belmonte, M., Chiono, V., Ferretti, C., Baino, F., Tonda-Turo, C., Vitale-Brovarone, C., Pashkuleva, I., Reis, R. L., Ciardelli, G. "Bioactive glass/polymer composite scaffolds mimicking bone tissue", Journal of Biomedical Materials Research: Part A, 100A(10), pp. 2654–2667, 2012. https://doi.org/10.1002/jbm.a.34205